Pseudospin-$\frac{3}{2}$ fermions, type-II Weyl semimetals, and critical Weyl semimetals in tricolor cubic lattices

Motohiko Ezawa
Department of Applied Physics, University of Tokyo, Hongo 7-3-1, 113-8656, Japan
(Received 11 September 2016; revised manuscript received 24 October 2016; published 16 November 2016)

Multiband touchings, such as three-band, six-band, and eight-band touchings, together with the emergence of high-pseudospin fermions were predicted recently at high-symmetry points in three-dimensional space. In this paper, we propose a simple cubic model whose unit cell contains three atoms. There are six bands in the system due to the spin degrees of freedom. The four-band and two-band touchings are realized at high-symmetry points, where we derive low-energy theories, demonstrating the emergence of pseudospin-3/2 fermions and Weyl fermions, respectively. Away from the high-symmetry points, we find critical Weyl fermions present exactly at the boundary between the type-I and type-II Weyl fermions. This critical Weyl fermion transforms into the type-I or type-II Weyl fermion once the magnetic field is applied.

DOI: 10.1103/PhysRevB.94.195205

I. INTRODUCTION

Dirac, Weyl, and Majorana fermions have attracted much attention in condensed-matter physics in views of topology and symmetry. They have a two-band touching with a linear dispersion. Dirac and Weyl fermions emerge in various materials, which are called Dirac and Weyl semimetals [1]. An interesting feature of Weyl semimetals is that they have a monopole charge in the momentum space, which protects the existence of the Weyl points topologically [2]. The type-II Weyl semimetal has attracted much attention recently [3–12], which emerges when the Weyl cone is highly tilted so that the Fermi surface consists of a pair of electron and hole pockets touching at the Weyl point. It is experimentally realized in $MoTe_2$ [13–17], LaAlGe [18], WTe_2 [19–22], $TaIrTe_4$ [23], $PtTe_2$ [24], and Ta_3S_2 [25].

Very recently, new types of fermions with multiband touching were proposed based on symmetry analysis as well as first-principles calculations, where three-band [26,27], six-band [26], and eight-band [26,28] touchings were reported at high-symmetry points. In particular, it is shown that the three-band touchings are well described by the fermions carrying the pseudospin 1. Furthermore, the eight-band touching has been proposed in antiperovskites to produce two sets of pseudospin-3/2 fermions [29]. On the other hand, the four-band touching is yet to be realized, although the existence of the pseudospin-3/2 fermion is discussed based on the symmetry analysis in the supplement of Ref. [26].

Motivated by these proposals on multiband touchings and fermions carrying higher pseudospins, we propose a lattice model possessing four-band and two-band touchings (Fig. 1). They are realized naturally in a lattice structure with the cubic symmetry where the unit cell contains three atoms (Fig. 2). We call it a tricolor cubic lattice. First, we derive the low-energy four-band theory at the high-symmetry points, which is shown to produce pseudospin-3/2 fermions having the angular momenta $j = (-3/2,-1/2,1/2,3/2)$. The bands have monopole charges $-3,-1,1,3$ at these points. Second, the two-band theory is described by the Weyl fermion. Furthermore, away from the high-symmetry points, we find a critical Weyl fermion, which resides at the exact boundary of the type-I and type-II Weyl fermions. They transform into type-I or type-II Weyl fermions once the magnetic field is applied.

This paper is organized as follows. In Sec. II, we propose a tricolor cubic lattice and the corresponding lattice Hamiltonian. In Sec. III, we show that four-band touching is realized in the band structure, where the effective Hamiltonian describes the pseudospin-3/2 fermion. In Sec. IV, we show the emergence of a critical Weyl fermion, which becomes type-I or type-II Weyl semimetals by applying a magnetic field.

II. MODEL HAMILTONIAN

We consider a cubic lattice as illustrated in Fig. 2(a). Though it looks complicated, the unit cell is quite simple. It contains three atoms represented by magenta, cyan, and yellow spheres [Fig. 2(b)]. Each color atom forms the body-center-cubic lattice. We call it a tricolor cubic lattice. The Brillouin zone is shown in Fig. 2(c). There are four high-symmetry points: $\Gamma(0,0,0)$, $P(\pi,\pi,\pi)$, $N(\pi,\pi,0)$, and $H(2\pi,0,0)$. Additionally, there are important points named $\Delta(\pi,0,0)$, $G(3\pi/2,\pi/2,0)$, $\Sigma(\pi/2,\pi/2,0)$, $\Lambda(\pi/2,\pi/2,\pi/2)$, $F(3\pi/2,\pi/2,\pi/2)$, and $D(\pi,\pi,\pi/2)$.

The main term of the lattice Hamiltonian is the hopping term along the bonds $\mathbf{d}_{ij} = \mathbf{r}_i - \mathbf{r}_j$ connecting a pair of the nearest-neighbor sites i and j in the tricolor cubic lattice [Fig. 2(a)]. The Hamiltonian has six bands due to the spin degrees of freedom. We introduce the spin-orbit interaction (SOI) preserving the cubic crystalline symmetry [30],

$$H_{\rm SO} = i\lambda \sum_{\langle i,j\rangle} c_i^\dagger [\sigma\cdot \mathbf{d}_{ij}] c_j, \tag{1}$$

with λ the coupling strength and $\sigma = (\sigma_x,\sigma_y,\sigma_z)$ the Pauli matrix for the spin. The six-band Hamiltonian reads $\hat{H}_6 = \sum_{\mathbf{k}} c^\dagger(\mathbf{k}) H_6(\mathbf{k}) c(\mathbf{k})$ in the momentum space, where

$$H_6(\mathbf{k}) = I_2 \otimes \begin{pmatrix} 0 & f_x & f_y^* \\ f_x^* & 0 & f_z \\ f_y & f_z^* & 0 \end{pmatrix} + \sigma_x \otimes \begin{pmatrix} 0 & g_x & 0 \\ g_x^* & 0 & 0 \\ 0 & 0 & 0 \end{pmatrix} + \sigma_y \otimes \begin{pmatrix} 0 & 0 & g_y^* \\ 0 & 0 & 0 \\ g_y & 0 & 0 \end{pmatrix} + \sigma_z \otimes \begin{pmatrix} 0 & 0 & 0 \\ 0 & 0 & g_z \\ 0 & g_z^* & 0 \end{pmatrix}, \tag{2}$$

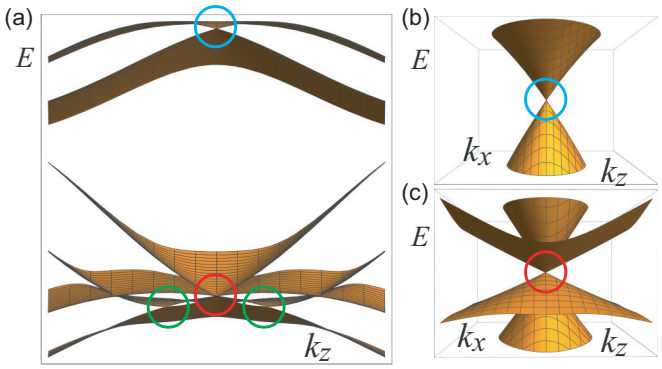

FIG. 1. Bird's eye view of the band structure near the P point. The horizontal plane is spanned by the k_z and k_x axes. The vertical axis is the energy $E = E(k_x,\pi,k_z)$. (a) Two-band (cyan circle) and four-band (red circle) touchings are observed at the P point. There appear other two-band touchings (green circle) off the P point. (b),(c) An enlarged portion of the two-band (four-band) touching indicates the emergence of (one) two Weyl cones at the P point.

with $f_\alpha = t\cos k_\alpha$, $g_\alpha = \lambda \sin k_\alpha$, $\alpha = x,y,z$, and the 2×2 unit matrix I_2. We remark that the SOI is zero ($g_\alpha = 0$) at the high-symmetry points Γ, P, N, H and also at the Δ point.

III. BAND STRUCTURE

The energy spectrum is obtained by diagonalizing the Hamiltonian. We show the band structure along the line Γ-Δ-H-G-N-Σ-Γ-Λ-P-F-H-F-P-D-N in Fig. 3 for typical values of the parameters t and λ. The four-band and two-band touchings are observed at various points in Fig. 3(b). The high-symmetry point P is typical, around which we show the bird's eye view of the band structure in Fig. 1.

The four-band touchings are protected by cubic crystalline symmetry and time-reversal symmetry. They occur at the high-symmetry points Γ, P, N, H and additionally at the Δ point. Hence, hereafter we count the point Δ as a member of the high-symmetry points. Let us explain how the four-band touching emerges. As shown in Fig. 3(a), in the absence of the SOI, the fourfold degeneracy is present due to the cubic crystalline symmetry at the high-symmetry points. Even by including the SOI, the bands never split at the time-reversal invariant momentum points, which implies the Kramers degeneracy. (In the present model this is realized since the SOI is zero at these points.) Consequently, the fourfold degeneracy without the SOI yields the four-band touching with the SOI at all the high-symmetry points [Fig. 3(b)].

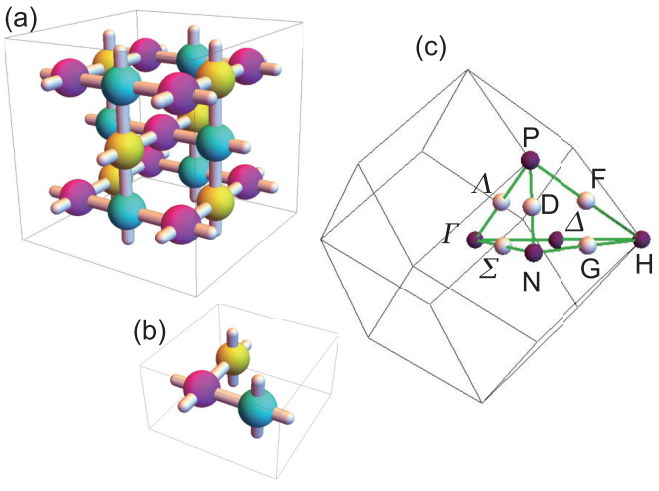

FIG. 2. Lattice structure and the Brillouin zone. (a) The lattice structure of a tricolor cubic lattice. (b) The unit cell contains three atoms, which are colored by magenta, cyan, and yellow. Each colored atom forms the body-center-cubic lattice. (c) The Brillouin zone and the high-symmetry points Γ, P, H, N, and Δ. The green bold lines show the cut along the Γ-Δ-H-G-N-Σ-Γ-Λ-P-F-H-F-P-D-N line.

To explore these touchings analytically, we diagonalize the Hamiltonian by a unitary transformation U,

$$U^{-1}H_6U = \nu t\,\mathrm{diag}(2,2,-1,-1,-1,-1), \tag{3}$$

at the high-symmetry points; $\nu = +$ for the Γ, N, and H points, and $\nu = -$ for the P and Δ points. The bands with the first two energies $2\nu t$ form a two-band touching, while those with the four energies $-\nu t$ form a four-band touching as in Fig. 3(b).

A. Four-band touching

First we construct the four-band model by way of

$$H_4(\mathbf{k}) = P_4U^{-1}H_6(\mathbf{k})U\,P_4, \tag{4}$$

where U is fixed by (3) while P_4 is the projection operator from the 6×6 Hamiltonian to the 4×4 Hamiltonian containing the four bands with the eigenenergies $-\nu t$. The four-band Hamiltonian is derived up to the linear order of k_α as

$$\nu H_4 = -t - \frac{\pi\lambda}{3}\begin{pmatrix} 0 & \eta\sqrt{3}k_z & 3ik_y & \eta\sqrt{3}k_x \\ \eta\sqrt{3}k_z & -2k_z & \eta\sqrt{3}k_x & 2k_x - ik_y \\ -3ik_y & \eta\sqrt{3}k_x & 0 & -\eta\sqrt{3}k_z \\ \eta\sqrt{3}k_x & 2k_x + ik_y & -\eta\sqrt{3}k_z & 2k_z \end{pmatrix}, \tag{5}$$

where $\eta = +$ for the Γ, P, N, H points and $\eta = -1$ for the Δ point. Here we have set the origin of the momentum $k_\alpha = 0$ at each high-symmetry point to investigate physics near the point. This Hamiltonian (5) is exactly diagonalizable,

$$E_j = \nu t \pm \frac{2j}{3}\lambda k, \quad k = |\mathbf{k}|, \tag{6}$$

which is independent of η, where $j = -3/2,-1/2,1/2,3/2$. The energy spectrum consists of two Weyl cones with velocities $\lambda/3$ and λ [Fig. 1(b)].

B. Pseudospin-3/2 fermion

The energy eigenvalues (6) as well as the eigenfunctions are the same as those of the pseudospin-3/2 Weyl fermion defined by

$$H_4 = \nu t + \tfrac{2}{3}\lambda\mathbf{k}\cdot\mathbf{J}, \tag{7}$$

where $\mathbf{J}$ is the pseudospin-3/2 operator. It implies that the Hamiltonian (5) is unitary equivalent to the system of the pseudospin-3/2 fermions.

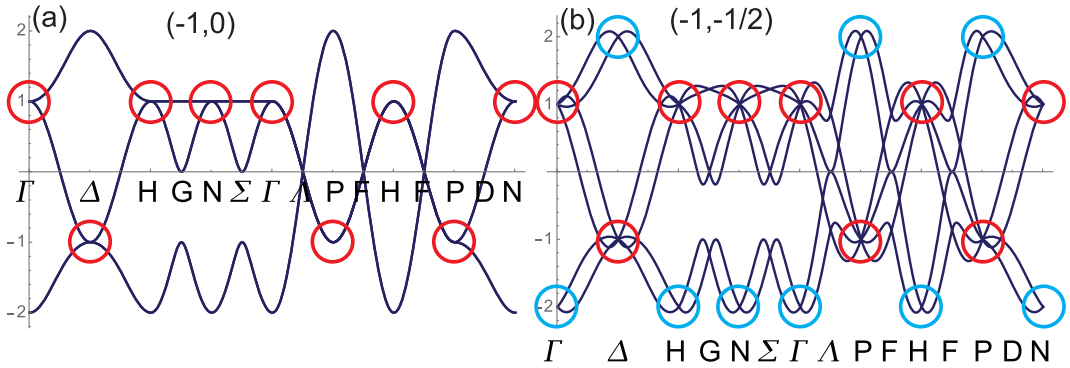

FIG. 3. Band structures of the six-band model. The band structure along the Γ-Δ-*H*-*G*-*N*-Σ-Γ-Λ-*P*- *F*-*H*-*F*-*P*-*D*-*N* line for typical values of parameters (t,λ) as indicated in the figures. (a) All energy bands are degenerate with respect to up and down spins when $\lambda = 0$. The fourfold degenerate points are marked by magenta circles. (b) The spin degeneracy is resolved by the SOI ($\lambda \neq 0$) except for the high-symmetry points (indicated by circles) where the SOI vanishes. Pseudospin-3/2 fermions (red) and Weyl fermions (cyan) emerge at various points.

A comment is in order with respect to the pseudospin-3/2 fermion. It has already been proposed in antiperovskites, where the effective low-energy Hamiltonian is written as [29,31]

$$H = m\tau_z + v_1\tau_x \mathbf{k}\cdot\mathbf{J} + v_2\tau_x \mathbf{k}\cdot\tilde{\mathbf{J}}. \tag{8}$$

It is an eight-band model due to the presence of another pseudospin degrees of freedom τ. Furthermore, this model has another operator $\tilde{\mathbf{J}}$ preserving the cubic symmetry, which introduces another velocity v_2. In general, it is impossible to obtain an exact energy spectrum of this Hamiltonian. However, if we set $m = 0$ and $v_2 = 0$ in this low-energy effective Hamiltonian, it is reduced to describe a double copy of the pseudospin-3/2 Weyl fermion, although the lattice structure is different from the one we are considering.

C. Monopoles

With the use of the eigenfunction, the Berry curvature is explicitly calculated for each band as [26]

$$\Omega(j) = i\nabla \times \langle\psi_j|\nabla\psi_j\rangle = j\frac{\mathbf{k}}{k}, \tag{9}$$

where j labels the band with $j = -3/2,-1/2,1/2,3/2$. In deriving the formula, we have used the fact $\frac{\partial\psi}{\partial r} = 0$. Since

$$\rho(j) = \frac{1}{2\pi}\iiint \nabla\cdot\Omega_j = 2j = -3,-1,1,3, \tag{10}$$

the Berry curvature of the band indexed by j describes a monopole with the monopole charge $2j$.

We note that with the use of the Matsubara Green function,

$$G(\mathbf{k}) = [i\omega - H(\mathbf{k})]^{-1}, \tag{11}$$

the Berry curvature is rewritten as

$$\Omega_i(j) = \frac{1}{6}\varepsilon_{i\mu\nu\rho}\langle\psi_j|\left[G\frac{\partial}{\partial k_\mu}G^{-1}G\frac{\partial}{\partial k_\nu}G^{-1}G\frac{\partial}{\partial k_\rho}G^{-1}\right]|\psi_j\rangle, \tag{12}$$

where $i = x,y,z$, while μ, ν, ρ run over 0, x, y, z with $k_0 = i\omega$ being the Matsubara frequency (ω: real). This formula has a merit that it can be used even in the presence of interactions [32–34].

IV. WEYL SEMIMETALS

We may also construct the two-band model by way of

$$H_2(\mathbf{k}) = P_2 U^{-1} H_6(\mathbf{k}) U P_2, \tag{13}$$

where P_2 is the projection operator from the 6×6 Hamiltonian to the 2×2 Hamiltonian containing the two bands with the eigenenergies $2vt$ in (3). The low-energy two-band model derived from this Hamiltonian describes Weyl fermions,

$$vH_2 = 2t + \tfrac{2}{3}\lambda(k_x\sigma_x - k_y\sigma_y - k_z\sigma_z). \tag{14}$$

We may verify the presence of monopole doublets ± 1 at the points Γ, N, H, and ∓ 1 at the points P, Δ, where the upper (lower) component dictates the monopole charge of the upper (lower) band. It is remarkable that Weyl fermions emerge naturally in the present three-dimensional tight-binding model. The Weyl semimetal is topologically protected as far as the two-band touching is intact.

We note that there also exist two-band touchings at the points G and Σ. However, since the effective theory is derived as

$$H_2 = \pm(-t + \lambda k_z\sigma_z), \tag{15}$$

they do not describe Weyl semimetals.

A. Critical Weyl semimetals

Two-band touchings emerge also at points which have no conventional names. See points marked by two green circles in Fig. 1(a) and Fig. 4(a1). We study the band structure near the points. Since they locate on the k_z axis, we derive the energy spectrum of the Hamiltonian H_4 by setting $k_x = k_y = 0$. It is given up to the order of k_z^2 as

$$vE_4(0,0,k_z) = -t \mp \lambda k_z + \frac{t}{2}k_z^2, \quad -t \mp \frac{\lambda}{3}k_z - \frac{t}{6}k_z^2. \tag{16}$$

We can check that these parabolic curves fit the results obtained by the six-band tight-binding model very well. There are two-band crossing points at $k_z = \pm\lambda/t$ with the energy $\pm(t + \lambda^2/2t)$: see Fig. 4(a2). In the vicinity of these points, we derive the two-band model with the use

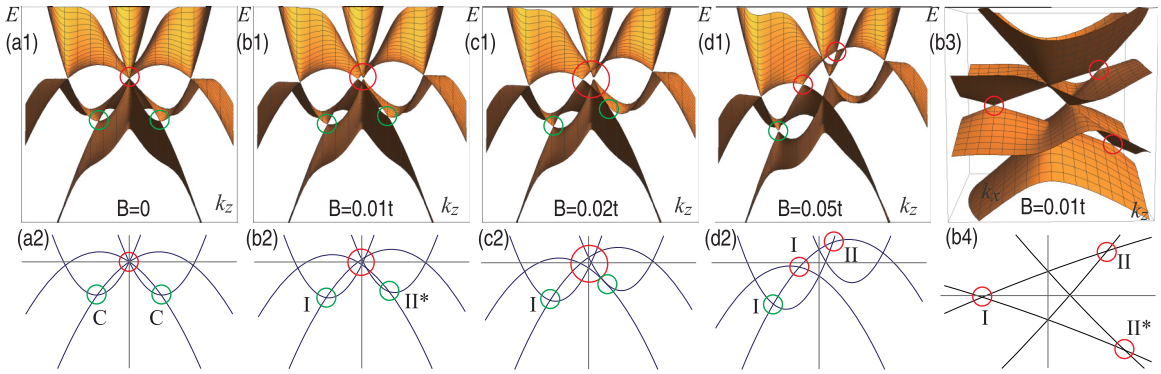

FIG. 4. Band structures in the vicinity of the P point. The horizontal axes are the k_z and k_x axes, while the vertical axis is the energy E. (a1)–(d1) The band structure without and with magnetic field B in the [001] direction. The value of B is given in the figures. Four-band touching (red circle) and two two-band touchings (green) are observed. (a2)–(d2) Four-band and two-band touchings occur along the k_z axis ($k_x = k_y = 0$). The cross sections of various surfaces are well approximated by parabolic curves. (b3) and (b4) show enlarged portions of the vicinity of the four-band touching in (b1) and (b2), respectively. Symbols C, I, and II stand for the critical, type-I, and type-II Weyl points, respectively. The points indicated by II* are identical to those in Figs. 5 and 6. (b2) shows that the four-band touching (red circle) is broken but the two two-band touchings (green) are not. The critical Weyl points in (a2) turn out to be type-I and type-II Weyl points in (b2). See also Fig. 5 for details. The pair of the type-II Weyl points (II*) in (c2) and (b4) are annihilated in (d2). See Fig. 6 for details.

of $k_z' = k_z \mp \lambda/t$,

$$vH_2^{\pm} = -t - \frac{\lambda^2}{2t} \mp \frac{1}{3}\lambda k_z' + \frac{t}{3}k_z'^2 + \frac{\lambda}{\sqrt{3}}\left(-k_x\sigma_x + k_y\sigma_y + \frac{1}{\sqrt{3}}k_z'\sigma_z\right) \pm \frac{t}{3}k_z'^2\sigma_z. \quad (17)$$

The energy spectrum along the k_z axis is given by

$$vE_2^{\pm}(0,0,k_z') = -t - \tfrac{\lambda^2}{2t} + \tfrac{t}{2}k_z'^2, \quad -t - \tfrac{\lambda^2}{2t} \mp \tfrac{2}{3}\lambda k_z' - \tfrac{t}{6}k_z'^2. \quad (18)$$

Interestingly, the linear order of k_z' is absent in the second energy spectrum. Consequently, they are critical Weyl semimetals between the type-I and -II Weyl semimetals.

B. Magnetic-field-induced type-II Weyl semimetals

We apply an external magnetic field ($B \neq 0$) in the [001] direction. The Hamiltonian is given by adding the term $B\sigma_z \otimes I_3$ to the Hamiltonian (2), where I_3 is the 3×3 unit matrix. There occurs the Zeeman split in the band structure as in Fig. 4.

With respect to the two-band touching (Weyl point), the only effect of the magnetic field is adding the Zeeman term $B\sigma_z$ to the Hamiltonian (14). It results in a shift of the Weyl point in the z direction, but the gap never opens.

On the other hand, the four-band touching is broken under the magnetic field. This is because it is protected by the time-reversal symmetry and the cubic symmetry.

Type-II Weyl fermions are produced in two different ways as the magnetic field is introduced. (i) First, as we remarked immediately above, there exist critical Weyl points in the vicinity of the four-band touching point [Figs. 4(a) and 5(a)]. They are turned into the type-I and type-II Weyl points [Figs. 4(b) and 5(b)]. (ii) Second, as the four-point touching is broken, there appear six two-point touchings in general as in Fig. 4(b4), among which we find type-II Weyl points.

We discuss the case (i): see Fig. 5. We study how the critical Weyl fermions are modified under a magnetic field. The crossing points are given by $k_z = \pm(\lambda + \sqrt{\lambda^2 + 12Bt})/2t$. In the linear order of B, the additional term to the two-band model (17) is

$$vH_2^{\pm} = B\left(\pm 1 + \frac{t}{\lambda}k_z' - \frac{2t}{\lambda}k_z'\sigma_z\right). \quad (19)$$

It transforms the two critical Weyl fermions into the type-I and type-II Weyl fermions. We note that a similar tilting of Weyl points in the Zeeman field has been discussed for the pseudospin-1 Weyl fermion in the supplement of Ref. [26].

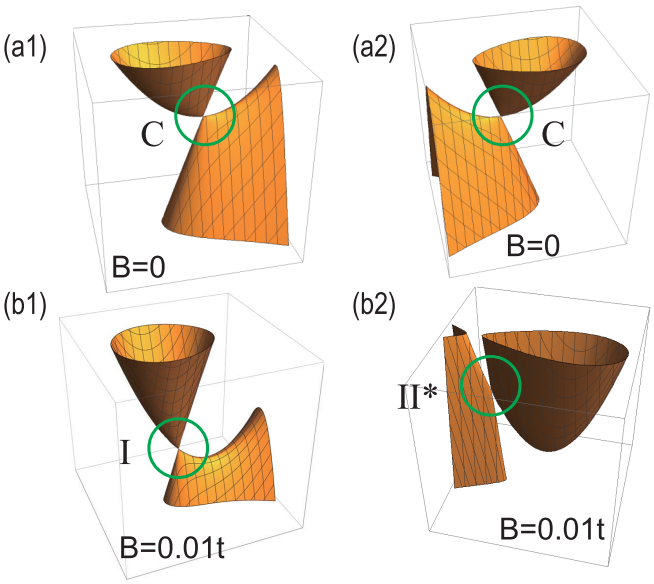

FIG. 5. Transition from the critical Weyl fermions to the type-I and type-II Weyl fermions. (a1),(a2) Critical Weyl points. (b1) Type-I Weyl point. (b2) Type-II Weyl point. They represent bird's eye views of the corresponding points in Figs. 4(a2) and 4(b2).

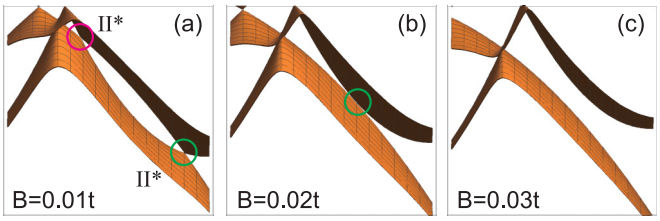

FIG. 6. Pair annihilation of two type-II Weyl fermions. (a) A bird's eye view of the type-II points marked II* in Figs. 4(b2) and 4(b4). (b) These two Weyl fermions merge at a critical magnetic field as in Fig. 4(c2). (c) They are annihilated beyond the critical field.

Next we discuss the case (ii): see Fig. 4(b3). In the four-band linear model, the energy spectrum along the k_z axis is given by $-vE = t \pm (\lambda k_z - B)$, $t \pm (\frac{1}{3}\lambda k_z - B)$. There are two-band crossings at $k_z = 3B/\lambda$. In the vicinity of this point, the two-band model is given by

$$H_2^{\pm} = \pm\Big[-t + 2B - \frac{2}{3}\lambda k_z' - \frac{\lambda}{\sqrt{3}}\Big(k_x\sigma_x - k_y\sigma_y - \frac{1}{\sqrt{3}}k_z'\sigma_z\Big)\Big], \quad (20)$$

with the energy spectrum

$$E_2^{\pm} = \pm\big(-t + 2B - \frac{2}{3}\lambda k_z' \pm \frac{1}{3}\lambda\sqrt{3k_x^2 + 3k_y^2 + k_z'^2}\big). \quad (21)$$

Since the tilt of the Weyl cone is larger than the velocity of the Weyl cone, they are type-II Weyl points.

We have mentioned the emergence of type-II Weyl points in two different ways. Interestingly, they are pair annihilated at $B = \pm\lambda^2/12t$ and disappear for $|B| > \lambda^2/12t$, as shown in Figs. 6(b) and 6(c), respectively.

V. DISCUSSION

We have shown that the four-band touching is realized in the tricolor cubic lattice. This four-band touching may be universal in the six-band system with the cubic symmetry and the time-reversal symmetry. There is the C_{3v} symmetry along the [111] axis in the cubic lattice. The C_{3v} symmetry has the irreducible representations (A_1, A_2, and E), where the E representation is the two-dimensional representation. If the E representation is realized, there is twofold degeneracy at the high-symmetry points such as the Γ and P points. Since the Γ and P points are the time-reversal invariant momentum, the Kramers degeneracy assures the four-band touching even when spin-orbit interactions are included. Our results indicate a possibility of multiband touching protected by the crystalline and the time-reversal symmetry.

ACKNOWLEDGMENTS

The author is very grateful to N. Nagaosa for many helpful discussions on the subject. He is also thankful for support by the Grants-in-Aid for Scientific Research from MEXT KAKENHI (Grants No. JP25400317 and No. JP15H05854).

[1] P. Hosur and X. L. Qi, C. R. Phys. **14**, 857 (2013).
[2] S. Murakami, New J. Phys. **9**, 356 (2007).
[3] A. A. Soluyanov, D. Gresch, Z. Wang, Q. S. Wu, M. Troyer, X. Dai, and B. Andrei Bernevig, Nature (London) **527**, 495 (2015).
[4] Y. Sun, S.-C. Wu, M. N. Ali, C. Felser, and B. Yan, Phys. Rev. B **92**, 161107 (2015).
[5] Z. Wang, D. Gresch, A. A. Soluyanov, W. Xie, S. Kushwaha, X. Dai, M. Troyer, R. J. Cava, and B. A. Bernevig, Phys. Rev. Lett. **117**, 056805 (2016).
[6] J. H. Pixley, D. A. Huse, S. Das Sarma, Phys. Rev. X **6**, 021042 (2016) .
[7] T. E. O'Brien, M. Diez, and C. W. J. Beenakker, Phys. Rev. Lett. **116**, 236401 (2016).
[8] Z.-M. Yu, Y. Yao, and S. A. Yang, Phys. Rev. Lett. **117**, 077202 (2016).
[9] A. Tamai, Q. S. Wu, I. Cucchi, F. Y. Bruno, S. Ricco, T. K. Kim, M. Hoesch, C. Barreteau, E. Giannini, C. Besnard, A. A. Soluyanov, and F. Baumberger, Phys. Rev. X **6**, 031021 (2016).
[10] S. Tchoumakov, M. Civelli, and M. O. Goerbig, Phys. Rev. Lett. **117**, 086402 (2016).
[11] C.-K. Chan, Y.-T. Oh, J. H. Han, and P. A. Lee, Phys. Rev. B **94**, 121106(R) (2016).
[12] M. Udagawa and E. J. Bergholtz, Phys. Rev. Lett. **117**, 086401 (2016).
[13] L. Huang, T. M. McCormick, M. Ochi, Z. Zhao, M. Suzuki, R. Arita, Y. Wu, D. Mou, H. Cao, J. Yan, N. Trivedi, and A. Kaminski, arXiv:1603.06482.
[14] K. Deng, G. Wan, P. Deng, K. Zhang, S. Ding, E. Wang, M. Yan, H. Huang, H. Zhang, Z. Xu, J. Denlinger, A. Fedorov, H. Yang, W. Duan, H. Yao, Y. Wu, S. Fan, H. Zhang, X. Chen, and S. Zhou, Nat. Phys. (2016).
[15] J. Jing, Z. K. Liu, Y. Sun, H. F. Yang, R. Rajamathi, Y. P. Qi, L. X. Yang, C. Chen, H. Peng, C.-C. Hwang, S. Z. Sun, S.-K. Mo, I. Vobornik, J. Fujii, S. S. P. Parkin, C. Felser, B. H. Yan, and Y. L. Chen, arXiv:1604.00139.
[16] A. Liang, J. Huang, S. Nie, Y. Ding, Q. Gao, C. Hu, S. He, Y. Zhang, C. Wang, B. Shen, J. Liu, P. Ai, L. Yu, X. Sun, W. Zhao, S. Lv, D. Liu, C. Li, Y. Zhang, Y. Hu, Y. Xu, L. Zhao, G. Liu, Z. Mao, X. Jia, F. Zhang, S. Zhang, F. Yang, Z. Wang, Q. Peng, H. Weng, X. Dai, Z. Fang, Z. Xu, C. Chen, and X. J. Zhou, arXiv:1604.01706.
[17] N. Xu, Z. J. Wang, A. P. Weber, A. Magrez, P. Bugnon, H. Berger, C. E. Matt, J. Z. Ma, B. B. Fu, B. Q. Lv, N. C. Plumb, M. Radovic, E. Pomjakushina, K. Conder, T. Qian, J. H. Dil, J. Mesot, H. Ding, and M. Shi, arXiv:1604.02116.
[18] S. Y. Xu, N. Alidoust, G. Chang, H. Lu, B. Singh, I. Belopolski, D. Sanchez, X. Zhang, G. Bian, H. Zheng, M.-A. Husanu, Y. Bian, S.-M. Huang, C.-H. Hsu, T.-R. Chang, H.-T. Jeng, A. Bansil, V. N. Strocov, H. Lin, S. Jia, and M. Z. Hasan, arXiv:1603.07318.

[19] C. Wang, Y. Zhang, J. Huang, S. Nie, G. Liu, A. Liang, Y. Zhang, B. Shen, J. Liu, C. Hu, Y. Ding, D. Liu, Y. Hu, S. He, L. Zhao, L. Yu, J. Hu, J. Wei, Z. Mao, Y. Shi, X. Jia, F. Zhang, S. Zhang, F. Yang, Z. Wang, Q. Peng, H. Weng, X. Dai, Z. Fang, Z. Xu, C. Chen, and X. J. Zhou, arXiv:1604.04218.

[20] Y. Wu, D. Mou, N. H. Jo, K. Sun, L. Huang, S. L. Bud'ko, P. C. Canfield, and A. Kaminski, Phys. Rev. B **94**, 121113 (2016).

[21] B. Feng, Y.-H. Chan, Y. Feng, R.-Y. Liu, M.-Y. Chou, K. Kuroda, K. Yaji, A. Harasawa, P. Moras, A. Barinov, W. G. Malaeb, C. Bareille, T. Kondo, S. Shin, F. Komori, T.-C. Chiang, Y. Shi, and I. Matsuda, arXiv:1606.00085.

[22] Y. Wang, E. Liu, H. Liu, Y. Pan, L. Zhang, J. Zeng, Y. Fu, M. Wang, K. Xu, Z. Huang, Z. Wang, H.-Z. Lu, D. Xing, B. Wang, X. Wan, and F. Miao, Nat. Commun. **7**, 13142 (2016).

[23] S. Khim, K. Koepernik, D. V. Efremov, J. Klotz, T. Forster, J. Wosnitza, M. I. Sturza, S. Wurmehl, C. Hess, J. van den Brink, and B. Buchner, Phys. Rev. B **94**, 165145 (2016).

[24] M. Yan, H. Huang, K. Zhang, E. Wang, W. Yao, K. Deng, G. Wan, H. Zhang, M. Arita, H. Yang, Z. Sun, H. Yao, Y. Wu, S. Fan, W. Duan, and S. Zhou, arXiv:1607.03643.

[25] D. Chen, L. X. Zhao, J. B. He, H. Liang, S. Zhang, C. H. Li, L. Shan, S. C. Wang, Z. A. Ren, C. Ren, and G. F. Chen, Phys Rev. B **94**, 174411 (2016).

[26] B. Bradlyn, J. Cano, Z. Wang, M. G. Vergniory, C. Felser, R. J. Cava, and B. A. Bernevig, Science **353**, aaf5037 (2016).

[27] G. Chang, S.-Y. Xu, S.-M. Huang, D. S. Sanchez, C.-H. Hsu, G. Bian, Z.-M. Yu, I. Belopolski, N. Alidoust, H. Zheng, T.-R. Chang, H.-T. Jeng, S. A. Yang, T. Neupert, H. Lin, and M. Z. Hasan, arXiv:1605.06831.

[28] B. J. Wieder, Y. Kim, A. M. Rappe, and C. L. Kane, Phys. Rev. Lett. **116**, 186402 (2016).

[29] T. H. Hsieh, J. Liu, and L. Fu, Phys. Rev. B **90**, 081112(R) (2014).

[30] M. Ezawa, New J. Phys. **16**, 065015 (2014).

[31] H. Isobe and L. Fu, Phys. Rev. B **93**, 241113 (2016).

[32] Z. Wang, X.-L. Qi, and S.-C. Zhang, Phys. Rev. Lett. **105**, 256803 (2010).

[33] Z. Wang and S.-C. Zhang, Phys. Rev. X **2**, 031008 (2012).

[34] V. Gurarie, Phys. Rev. B **83**, 085426 (2011).